ARTICLE

doi:10.1038/nature14003

Structure of the *V. cholerae* Na^+-pumping NADH:quinone oxidoreductase

Julia Steuber[1], Georg Vohl[2,3]*, Marco S. Casutt[2]*, Thomas Vorburger[1], Kay Diederichs[4] & Günter Fritz[2]

NADH oxidation in the respiratory chain is coupled to ion translocation across the membrane to build up an electrochemical gradient. The sodium-translocating NADH:quinone oxidoreductase (Na^+-NQR), a membrane protein complex widespread among pathogenic bacteria, consists of six subunits, NqrA, B, C, D, E and F. To our knowledge, no structural information on the Na^+-NQR complex has been available until now. Here we present the crystal structure of the Na^+-NQR complex at 3.5 Å resolution. The arrangement of cofactors both at the cytoplasmic and the periplasmic side of the complex, together with a hitherto unknown iron centre in the midst of the membrane-embedded part, reveals an electron transfer pathway from the NADH-oxidizing cytoplasmic NqrF subunit across the membrane to the periplasmic NqrC, and back to the quinone reduction site on NqrA located in the cytoplasm. A sodium channel was localized in subunit NqrB, which represents the largest membrane subunit of the Na^+-NQR and is structurally related to urea and ammonia transporters. On the basis of the structure we propose a mechanism of redox-driven Na^+ translocation where the change in redox state of the flavin mononucleotide cofactor in NqrB triggers the transport of Na^+ through the observed channel.

Electrogenic NADH:ubiquinone oxidoreductases are central components of the respiratory chain in mitochondria and bacteria. These enzymes are integral membrane proteins that oxidize cytoplasmic NADH and reduce ubiquinone located in the membrane. The energy released by this redox reaction is used by complex I and the Na^+-NQR to pump ions across the membrane, thus generating the electrochemical gradient that is essential for all living organisms[1]. Although these two membrane protein complexes catalyse a very similar reaction, their basic architecture is completely different. The Na^+-NQR is composed of the six subunits NqrA, B, C, D, E, F and has been reported to contain a unique set of cofactors: one FAD, a [2Fe–2S] cluster, two covalently bound flavin mononucleotide (FMN), riboflavin and a tightly bound ubiquinone[2–4]. The Na^+ gradient generated by the Na^+-NQR is essential for *Vibrio cholerae* for being infectious, for example, by driving its monopolar flagellum required for motility. Moreover, the activity of Na^+-NQR is linked to the expression of virulence factors, and inhibition of Na^+-NQR decreases toxin production[5]. Genes for the Na^+-NQR were identified in many pathogenic bacteria and have no eukaryotic homologue, designating the enzyme as a probable drug target in antibacterial therapy. Interestingly, four out of six subunits, NqrB, NqrC, NqrD and NqrE, are homologous to subunits of the so-called RNF (*Rhodobacter* nitrogen fixation) complex present in widely different groups of prokaryotes[6] (Extended Data Figs 1, 2). The high similarity over four subunits suggests that the core machinery for Na^+ translocation is identical in both respiratory complexes. To date no structural information is available for the Na^+-NQR or the RNF complex. Here we report on the crystal structure of the entire Na^+-NQR complex at 3.5 Å resolution (Extended Data Table 1). To gain further insights we complemented the low-resolution information with high-resolution structural data on several subunits, by determining the structures of the major soluble domains of subunits NqrA, NqrC and NqrF at 1.60 Å, 1.70 Å and 1.55 Å resolution, respectively.

Overall structure

The entire complex has dimensions of 87 Å × 138 Å × 52 Å (Fig. 1). The transmembrane part of Na^+-NQR is mainly formed by the subunits NqrB, NqrD and NqrE, which are integral membrane proteins with small domains in the cytoplasm or periplasm (Extended Data Fig. 3). NqrA, NqrC and NqrF are large hydrophilic subunits with the latter two anchored via a single transmembrane helix in the cytoplasmic membrane. The hydrophilic subunits NqrA and NqrF protrude into the cytoplasm, whereas NqrC resides in the periplasm (Fig. 1). NqrA, which lacks transmembrane helices, is tightly bound to NqrB, forming a complex with a large interaction surface (Fig. 1 and Extended Data Fig. 4a). Subunits NqrD and NqrE form a central structural unit that interacts with subunit NqrB on one side and the transmembrane helices of NqrC and NqrF on the opposed side (Extended Data Fig. 3d, e).

The hydrophilic subunits in the cytoplasm

NqrA consists of four domains (Extended Data Fig. 4b, c). The amino-terminal domain (residues 28–100) exhibits similarity to a biotin carboxyl carrier domain. It is followed by a Rossmann-fold domain (102–254), an ubiquitin-like domain (residues 258–329), and a carboxy-terminal helical domain (376–446). At the sequence level, NqrA shows no resemblance to proteins of known structure. However, a DALI search[7] revealed an unexpected structural similarity with subunit Nqo1 of bacterial complex I[8]. Despite their distinct function, the similarity between NqrA and Nqo1 is remarkable with a root-mean-square deviation (r.m.s.d.) of 3.9 Å over 234 Cα positions (Extended Data Fig. 4d). The carboxy-terminal helical domain of NqrA shows similarity to a 2[4Fe–4S] cluster ferredoxin fold but does not contain an FeS centre. Although NqrA is structurally similar to subunit Nqo1 of complex I, there is no overlap at the functional level. Whereas Nqo1 binds an FMN cofactor in the Rossmann fold, NqrA contains no cofactor and it has been proposed that the subunit lost its cofactors during evolution of Na^+-NQR[9]. Although we have recently mapped the ubiquinone interaction site in NqrA by photo-affinity labelling and NMR[4,10], we could not observe this cofactor in the low-resolution electron density of the entire Na^+-NQR. NqrA comprises a deep solvent-accessible cavity that is formed by residues of the Rossmann-fold domain and the ubiquitin-like domain that is large enough to accommodate ubiquinone. NqrA forms major contacts with NqrB via its N and C

[1]Department of Microbiology, Garbenstrasse 30, University of Hohenheim, 70599 Stuttgart, Germany. [2]Institute for Neuropathology, University of Freiburg, Breisacher Strasse 64, 79106 Freiburg, Germany. [3]Hermann-Staudinger-Graduate school, University of Freiburg, Hebelstrasse 27, 79104 Freiburg, Germany. [4]Department of Biology, University of Konstanz, Universitätsstrasse 10, 78457 Konstanz, Germany.
*These authors contributed equally to this work.

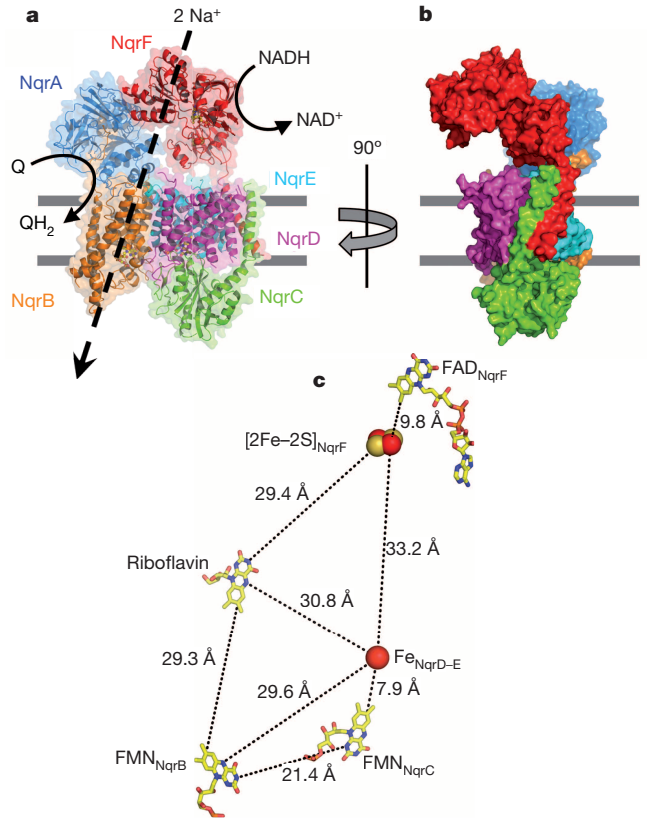

Figure 1 | Overall structure of Na^+-NQR. **a**, **b**, Na^+-NQR is composed of six subunits, NqrA–NqrF. While NqrA (blue) contains no transmembrane helix, NqrB (orange), NqrD (magenta) and NqrE (cyan) are integral membrane proteins. NqrF (red) and NqrC (green) are anchored in the cytoplasmic membrane by a single transmembrane helix. The membrane plane is indicated by grey lines. NADH oxidation occurs at NqrF and ubiquinone (Q) has been shown to bind to NqrA. The energy liberated is used to translocate two Na^+ per NADH oxidized[34]. **b**, The solvent accessible surface of Na^+-NQR is shown. **c**, The arrangement of the redox cofactors in Na^+-NQR. Edge-to-edge distances of the cofactors are indicated by broken lines.

termini. The N-terminal residues 38–51 of NqrB reside in a deep groove of NqrA (Extended Data Fig. 4a). At the C terminus of NqrB, transmembrane helix 10 is elongated and protrudes into the cytoplasm, forming contacts with the C-terminal domain and the Rossmann-fold domain of NqrA.

NqrF consists of two major hydrophilic domains anchored by a single transmembrane helix to the Na^+-NQR complex. The N-terminal ferredoxin-like domain following the transmembrane helix harbours a [2Fe–2S] cluster and is located proximal to the membrane, whereas the C-terminal FAD-binding domain resides remote of the membrane (Fig. 1). The linker regions between the transmembrane helix, the ferredoxin-like domain and the FAD-binding domain were barely visible in the electron density, suggesting a high degree of flexibility. The FAD-binding domain of NqrF is reminiscent to the ferredoxin-$NADP^+$ reductase-type flavoproteins and represents the NADH-oxidizing unit of Na^+-NQR. In contrast to NqrA that exhibits multiple and large contacts to the integral membrane subunit NqrB, NqrF does not interact with the membrane subunits. Neither the FAD-binding nor the ferredoxin-like domain show any contact with the NqrB, NqrD or NqrE. The ferredoxin-like domain resides in a distance of 10 Å to NqrE and the FAD-binding domain in a distance of 25 Å to NqrD, leaving a large gap between the integral membrane subunits NqrD–E and NqrF. This spatial arrangement suggests that the hydrophilic domains of NqrF might move towards the membrane subunits of the complex, with the linker regions of NqrF acting as hinges.

NqrB harbours a Na^+ channel

NqrB comprises 10 transmembrane helices and the arrangement of the helices suggests that the subunit has originally evolved from gene duplication (Extended Data Fig. 3a). Search for structural homologues revealed that NqrB is homologous to urea and ammonium transporters from prokaryotes and eukaryotes. Despite the low sequence identity (5–12%), the structural similarity is rather high. In structural alignments of NqrB with a urea transporter from *Bos taurus* (PDB code 4EZC)[11], 205 residues were aligned with an r.m.s.d. of 3.7 Å for the Cα positions (Extended Data Fig. 5a). Correspondingly, structural alignment with ammonium transporters from different species revealed an r.m.s.d. of 3.6 Å for 210 residues[12,13] (Extended Data Fig. 5b). Both urea transporter and ammonia transporter mediate the transport of small solutes[11,14] across the membrane through a central cavity. The similarity of the three different membrane proteins is intriguing and suggests that they have evolved from a common ancestor that transported positively charged ions or molecules. In NqrB the central helices I, III, VI and VIII form a membrane-spanning channel (Fig. 2a, b). However, when compared to the urea transporter the channel in NqrB is narrowed by a relocation of the rather short helix VIII by approximately 5 Å towards the centre of the protein (Extended Data Fig. 5a, b). Several residues located on this helix appear to be crucial for the transport of Na^+ across the membrane. The channel opens at the cytoplasmic aspect of NqrB, forming a wide vestibule that displays a negatively charged surface (Extended Data Fig. 5c). Residue Asp 346 of NqrB is located at the bottom of this vestibule (Fig. 2c), and mutational studies have suggested that this aspartic residue is involved in Na^+ transport[15]. At a position halfway through the membrane the channel narrows sharply and the access to the second half of the channel, which opens to the periplasm, is blocked by side chains of hydrophobic residues: Phe 338 and Phe 342 located on helix VIII, Ile 164, Leu 165 and Leu 168 on helix III, and Val 64 of helix I (Fig. 2c, d). Rotation of the side chain of either Phe 342 or Ile 164 would completely block the observed channel. After this constriction the channel opens widely, forming a large cavity with an exit site to the periplasmic aspect of NqrB. In this arrangement Na^+ ions can enter the channel from the cytoplasmic or periplasmic side, but cannot pass the constriction. Interestingly, the cytoplasmic half-channel is negatively charged, whereas the periplasmic half-channel is positively charged (Extended Data Fig. 5c). This asymmetric charge distribution in the two half-channels might cause an enrichment of Na^+ ions in the cytoplasmic half versus the periplasmic half, facilitating the directional transport of the cations.

As a major difference to the urea and ammonium transporter proteins, NqrB comprises an additional periplasmic domain that harbours an FMN cofactor that is covalently linked via its phosphate group to Thr 236. This FMN-binding domain is assembled by insertions into the regions connecting the transmembrane helices I/II, V/VI and VII/VIII of NqrB and encompasses a total of 120 residues. The FMN itself is deeply buried in the protein (Fig. 2a) with the isoalloxazine moiety located within the transmembrane region and the cavity around the FMN connected to the periplasmic Na^+ half-channel (Extended Data Fig. 5c).

Thus, NqrB represents a molecule that preserved the basic architecture of a transporter but has acquired an additional and completely different function as a redox protein. An opening of the Na^+ channel must be coupled to changes in the redox state of the Na^+-NQR complex and it appears reasonable that a change of the redox state of FMN in NqrB triggers Na^+ translocation as proposed previously on the basis of kinetic data[16].

A Fe site in NqrD–E

The localization of the Na^+ channel in NqrB raises the question of the function of the other integral membrane subunits NqrD and NqrE. Structurally, both subunits are closely related and very likely the result of a gene duplication. Each subunit comprises six transmembrane helices connected by short loop regions in the cytoplasm and periplasm (Extended Data Figs 1a, b and 3b, c). As a major difference the transmembrane helices of both subunits exhibit an inverted path through the

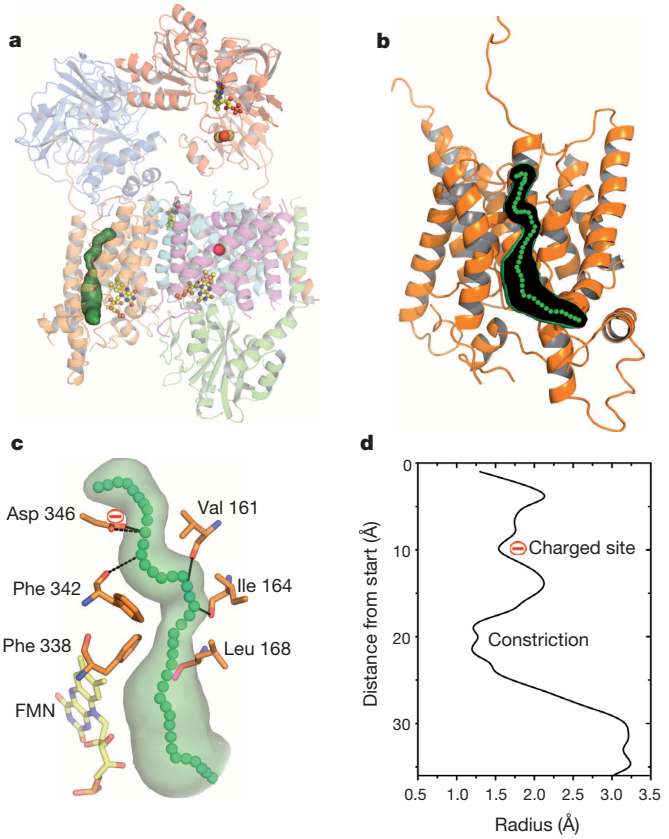

Figure 2 | Subunit NqrB harbours a Na^+-channel. **a**, Analysis of the transmembrane subunits with CAVER revealed a hydrophilic channel (green) in subunit NqrB. **b**, Close-up view of the channel in NqrB. Transmembrane helix I is removed for clarity. The green spheres indicate the proposed path of the Na^+ through NqrB. **c**, Key residues of the putative Na^+ channel. The negatively charged side chain of Asp 346 can coordinate Na^+ at the entry of the channel. The backbone carbonyl residues of Val 161, Ile 164 and Leu 168 located on transmembrane helix III can coordinate the Na^+ on the predicted path. **d**, Ile 164, Leu 168 and on the opposite site Phe 338 and Phe 342 located on transmembrane helix VIII narrow the channel, forming a constriction.

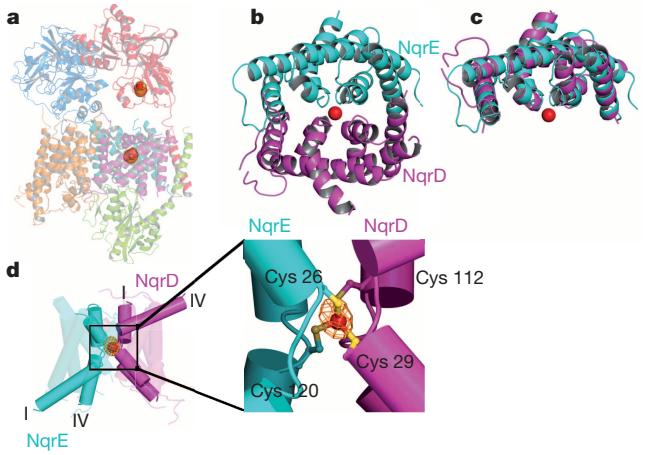

Figure 3 | Subunits NqrD and NqrE contain a novel Fe centre. **a**, Two strong peaks in the anomalous difference map shown in orange at 5σ were detected. The first peak was assigned to the [2Fe–2S] centre in NqrF and the second peak in the centre between subunit NqrD and NqrE. The [2Fe–2S] cluster and the Fe are shown as spheres. **b**, **c**, Top view of subunits NqrD (magenta) and NqrE (cyan). NqrD and NqrE form a symmetrical dimer. Both subunits are related by a two-fold axis. The centre of this unusual dimer is formed by transmembrane helices I and IV of NqrD and NqrE, which form two half-helices instead of a continuous transmembrane helix. **d**, Approximately in the centre of the membrane plane the helices unfold and four Cys residues originating from each helix coordinate the Fe centre. The anomalous difference map is shown at 8σ.

membrane. NqrD and NqrE assemble into a symmetrical entity where both subunits are related by a rotation of 180° around a two-fold axis located in the centre of the membrane (Fig. 3b, c). Transmembrane helices I and IV from both subunits form the core of the NqrD–E unit. These four transmembrane helices are organized as half-helices with each half-helix tilted by approximately 45° with respect to the membrane plane. The linker regions of the four central helices meet in the centre, thereby forming a core structure resembling an hourglass. In the centre of this core unit a strong anomalous signal was observed originating from a Fe centre (Fig. 3a, d). The identity of Fe was confirmed by comparison of the intensity of the peak at different wavelengths (Extended Data Table 2). Four cysteine residues originating from each of the core helices coordinate the Fe via the thiol group of the side chain. It appears that the four transmembrane helices harbouring the cysteine residues unwind in the centre of the membrane to accommodate for iron coordination (Fig. 3b, d). The coordination and localization of the single Fe in the membrane region of Na^+-NQR is unprecedented and represents a so far unknown redox cofactor of Na^+-NQR.

NqrC represents a new type of flavoprotein

NqrC contains, like NqrB, a covalently bound FMN that is linked via a phosphoester to the side chain of Thr 225 (ref. 17). There is a debate on the topology of NqrC. On the basis of PhoA fusions it was proposed that NqrC resides in the cytoplasm[18], whereas the insertion of the covalently bound FMN into NqrC in the periplasm suggested a periplasmic localization[19]. Here we show that NqrC resides in the periplasm (Figs 1 and 4). The single transmembrane helix that anchors this hydrophilic subunit in the membrane elongates to a long helix that is part of the fold of NqrC. Structurally, NqrC is not related to any known protein family. The fold of NqrC comprises a central five-strand β-sheet that is sandwiched on both sides by two helices from the N terminus and C terminus. At the periplasmic aspect, NqrC plunges into a deep cavity of the NqrD–E unit (Fig. 4a, b). The FMN of NqrC is covalently attached via a phosphoester bond to the oxygen of the side chain of Thr 225 located in a helix of the C terminus (Fig. 4b). The isoalloxazine moiety of the FMN resides in an open pocket and more than half of the isoalloxazine plane protrudes out from the NqrC protein matrix to be embedded in the cavity formed by NqrD and NqrE (Fig. 4b, c).

Riboflavin binding site

Deletion of subunit NqrB leads to the loss of riboflavin in Na^+-NQR, indicating that riboflavin is bound to this subunit[20]. After completion of the model of Na^+-NQR we did not observe any additional difference electron density inside NqrB that could encompass a riboflavin cofactor. An unbiased analysis of the $F_o - F_c$ difference map around the entire Na^+-NQR by automatic fitting[21] revealed a large patch of $F_o - F_c$ density at the interface between NqrB and NqrE. The aromatic isoalloxazine moiety fits well into the $F_o - F_c$ density (Extended Data Fig. 6), whereas other candidates, like for example ubiquinone, are too small. The riboflavin-binding site is located in the transmembrane region but close to the cytoplasmic aspect, suitable for electron transfer to ubiquinone located in NqrA[4,10].

Electron transfer pathway

In total there are seven redox cofactors described to be present in Na^+-NQR: four flavin cofactors, one [2Fe–2S] cluster, the Fe site in NqrD–E described here for the first time (Fig. 1c), and a tightly bound ubiquinone. Edge-to-edge and centre-to-centre distances of the redox cofactors are listed in Extended Data Table 3. NADH is oxidized in a two-electron step at the FAD of subunit NqrF and electrons are transferred one-by-one from FAD to the [2Fe–2S] cluster residing at an edge-to-edge distance of 9.8 Å in the N-terminal domain of NqrF. Mutational and fast

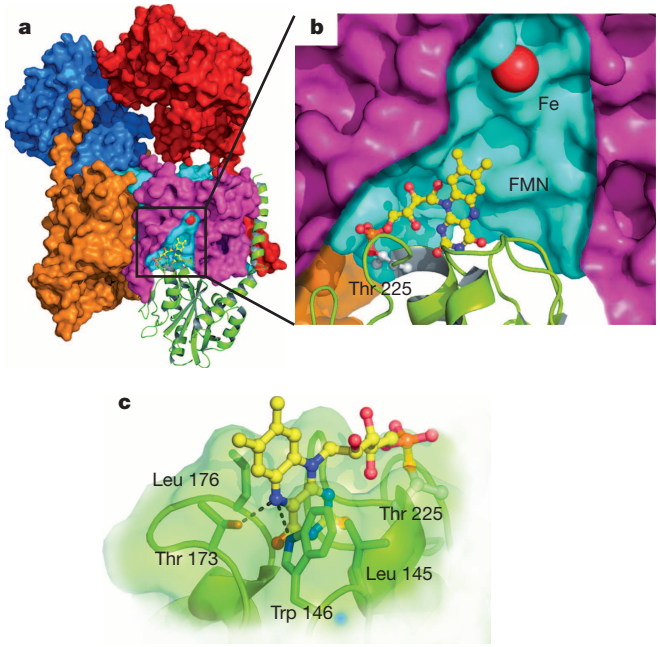

Figure 4 | Subunit NqrC exhibits a new flavoprotein fold and FMN-binding motif. **a**, A part of subunit NqrD (magenta) is removed to show the localization of NqrC (green). **b**, The FMN_{NqrC} is covalently bound via a phosphoester bond between the ribityl phosphate and the Thr 225 side chain. The distance between the FMN and the Fe centre in NqrD–E is just 8 Å, with the C7 and C8 methyl groups of the isoalloxazine pointing directly to the Fe centre. **c**, NqrC binds FMN in an unprecedented way; only the pyrimidine moiety of isoalloxazine is embedded in the protein matrix with the benzene moiety protruding from the surface. The aromatic isoalloxazine is sandwiched between Leu 145 and Leu 176. Additional hydrogen bonds by the side chains of Trp 146 and Thr 173 to N5 of FMN might stabilize its position and tune the redox potential. A further hydrogen bond between O4 of the ribityl and N1 might stabilize the radical state of the FMN.

kinetics data indicate that the electrons are subsequently transferred to FMN_{NqrC}[16], and via FMN_{NqrB}, and $riboflavin_{NqrB}$ finally to ubiquinone. However, FMN_{NqrC} resides in the periplasm and the electrons have to cross the cytoplasmic membrane, making direct electron transfer from NqrF to NqrC very unlikely. The Fe site in the core of subunits NqrD and NqrE is well suited to bridge electron transfer between NqrF and NqrC. The proposed electron transfer pathway can be summarized in the following scheme:

$$NADH \rightarrow FAD_{NqrF} \rightarrow [2Fe-2S]_{NqrF} \rightarrow Fe_{NqrD-E} \rightarrow$$

$$FMN_{NqrC} \rightarrow FMN_{NqrB} \rightarrow Riboflavin_{NqrB} \rightarrow Q_{NqrA}$$

However, several distances between the redox centres in the proposed electron transfer pathway are too large for fast electron transfer[22] and are not in agreement with measured rates of Na^+-NQR[16,23]. The edge-to-edge distance between the [2Fe–2S] cluster in NqrF and the Fe in NqrD–E is 33.4 Å, whereas the isoalloxazine moiety of FMN_{NqrC} is located in very close proximity to the Fe_{NqrD-E} with an edge-to-edge distance of just 7.9 Å. During turnover the N-terminal domain of NqrF has to undergo a large conformational change decreasing the gap between $[2Fe–2S]_{NqrF}$ and Fe_{NqrD-E} to allow for efficient electron transfer. Such a conformational change has been observed so far only in bc_1 complex of the respiratory chain. The [2Fe–2S] cluster bearing subunit of bc_1 complex switches between two positions to shuttle electrons from ubiquinol to cytochrome c_1[24]. In subunit NqrF the transmembrane helix, the [2Fe–2S] domain and the FAD-binding domain are connected by flexible linkers, enabling a rotational movement of the [2Fe–2S] domain towards the membrane plane and shortening the distance between $[2Fe–2S]_{NqrF}$ and Fe_{NqrD-E}.

From FMN_{NqrC} electron transfer proceeds to the covalent FMN in NqrB. FMN_{NqrB} is bound to Thr 236 and, like FMN_{NqrC}, it is located at the periplasmic side of the complex, close to the hydrophobic core of NqrB. The edge-to-edge distance between FMN_{NqrC} and FMN_{NqrB} is 21.4 Å, but might decrease to approximately 15 Å according to electron paramagnetic resonance (EPR) analysis of spin–spin interactions between the radical state of both FMN cofactors[25]. Both, FMN_{NqrC} and FMN_{NqrB} are well shielded from the solvent in order to minimize side reactions in the periplasm. Riboflavin was localized at an edge-to-edge distance of 29.3 Å to FMN_{NqrB} in the hydrophobic/hydrophilic transition zone at the cytoplasmic side of NqrB. Again this distance is too large for fast electron transfer. The observed electron transfer from FMN_{NqrB} to $riboflavin_{NqrB}$ requires either a movement of FMN or riboflavin in NqrB. The covalent attachment of FMN to Thr 236 makes a movement unlikely, suggesting the possibility for a switch involving $Riboflavin_{NqrB}$.

Taking into account the data from previous studies and the now available structural data, two passages of the electron across the cytoplasmic membrane must be predicted. Such a pathway has implications on the mechanism and energetics of Na^+ translocation as discussed later. Moreover, the architecture of the Na^+-NQR reveals that NqrB, NqrC, NqrD and NqrE comprise the core machinery of the pump and carry the redox cofactors required for redox-driven Na^+ translocation. Subunits NqrA and NqrF represent electron input and electron output devices and are substituted in the RNF complex by functionally different subunits. Noteworthy, NqrB, NqrC, NqrD and NqrE are highly homologous to subunits RnfD, RnfG, RnfA and RnfE of the RNF complex[6,26] (Extended Data Figs 1 and 2), underlining their central function, and strongly suggesting that changes in the redox state of cofactors within these subunits must be critically coupled to Na^+ translocation events.

Mechanism of Na^+ translocation

On the basis of the available data we developed a model of coupling between electron transfer and Na^+ translocation in Na^+-NQR. Two general but different mechanisms describing the coupling of electron transfer to Na^+ transport in Na^+-NQR have been proposed previously. In the first model a mechanism of thermodynamic coupling where Na^+ binds to a cofactor dependent on its redox state was suggested[27]. In such a scenario co-translocation of an electron and Na^+ across the membrane would be electroneutral and therefore energetically much less unfavourable. This model predicts that the redox potentials of cofactors involved are dependent on the presence of the coupling ion. However, so far there was no clear hint for Na^+-dependent changes in redox potential[28,29]. In a second model no direct interaction of Na^+ with a redox cofactor occurs and Na^+ translocation is mediated by redox-dependent conformational changes. The data of previous studies and the data provided here support the latter model and link distinct electron transfer steps to ion translocation events.

The oxidation of NADH at FAD_{NqrF} and the subsequent electron transfer to $[2Fe–2S]_{NqrF}$ (Fig. 5a) are presumably not coupled to ion translocation events, as supported by kinetic data[30] showing that both reactions are independent on the presence of the coupling ion Na^+. The transition of an electron from $[2Fe–2S]_{NqrF}$ to Fe_{NqrD-E} triggers most likely binding of a Na^+ in the negatively charged binding pocket in NqrB that opens to the cytoplasm (Fig. 5a). This is in agreement with kinetic data showing that electron transfer from $[2Fe–2S]_{NqrF}$ to FMN_{NqrC} is dependent on Na^+ and triggers capture of Na^+[16,31]. Both, the Fe_{NqrD-E} and the Na^+ binding site at Asp 346 in the pocket of NqrB are about half-way through the membrane, representing an electroneutral and energetically favoured relay station of the transport. The conformational change in NqrF required for electron transfer between $[2Fe–2S]_{NqrF}$ to Fe_{NqrD-E} might be coupled to subtle changes in NqrB facilitating access and binding of Na^+. The short distance between Fe_{NqrD-E} and FMN_{NqrC} promotes a very fast electron transfer in the subsequent step that is presumably not coupled to the comparable slow ion translocation events. It is reasonable to assume that the next electron transfer step from FMN_{NqrC} to FMN_{NqrB} triggers the occlusion of the Na^+ in NqrB (Fig. 5a). In

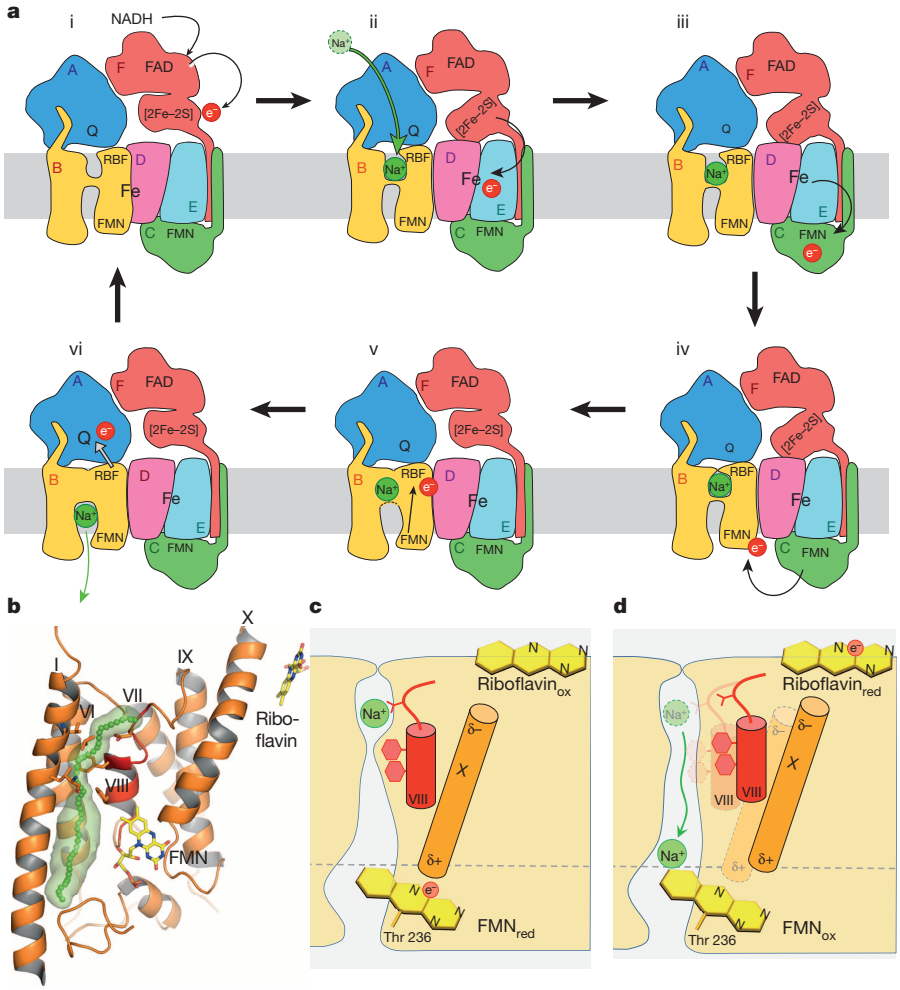

Figure 5 | Mechanism of redox-driven Na^+ translocation. **a**, Model for coupling between electron transfer and Na^+ translocation. NADH is oxidized at FAD_{NqrF} that mediates single electron transfer to $[2Fe–2S]_{NqrF}$ (i). A conformational change in NqrF is required to transfer the electron to the $Fe_{NqrD–E}$. This step might facilitate concomitant Na^+-binding in the cytoplasmic half-channel of NqrB (ii). Subsequently the electron is transferred to FMN_{NqrC} (iii), and FMN_{NqrB} (iv). The latter step presumably triggers the occlusion of Na^+. Electron transfer from FMN_{NqrB} to $riboflavin_{NqrB}$ (RBF; v) leads to an opening of the constriction and Na^+ is released to the periplasmic half channel of NqrB. The release might be dependent on the reduction of ubiquinone (vi). **b**–**d**, The redox state of FMN_{NqrB} controls the position of helix X pointing with the positive end of the helix dipole directly towards the N5. Electron transfer from FMN_{NqrB} to $riboflavin_{NqrB}$ releases helix X that will move along with helix VIII. The shift of Phe 338 and Phe 342 located on helix VIII of NqrB will open the constriction and trigger translocation of the Na^+ to the periplasmic half-channel. The wide periplasmic half-channel is most likely filled with water molecules, which will immediately form a water shell around the Na^+.

agreement with this assumption, EPR-based distance measurements between the one-electron-reduced FMN cofactors point towards substantial Na^+-dependent conformational changes[25]. The energy of this step might be further used to strip off the water shell of the Na^+ and coordinate the ion by oxygen atoms deriving from the protein backbone and from the NqrB Asp 346 side chain. The redox state of flavin cofactors is known to control protein function by acting as a redox switch inducing conformational changes[32,33]. In NqrB the one-electron reduced state of FMN_{NqrB} might pull transmembrane helix X pointing with its helix dipole directly towards the N5 of FMN_{NqrB} (Fig. 5b, c). Transmembrane helix X of NqrB is in close contact with the short transmembrane helix VIII carrying residues Phe342 and Phe338, which constricts the proposed Na^+ channel (Figs 2c and 5b, c). Any movement of helix X would induce a movement of helix VIII as well. Previous studies[16] put forward that electron transfer from FMN_{NqrB} to $riboflavin_{NqrB}$ is coupled to the release of Na^+ to the periplasm. Oxidation of the FMN_{NqrB} radical to the uncharged form might lead to the loss of the interaction between N5 of FMN_{NqrB} and the helix dipole, thereby releasing helix X. Concomitantly, helix VIII moves along with helix X. This movement opens the constriction involving residues Phe 338 and Phe 342 and triggers translocation of the Na^+ to the periplasmic half-channel (Fig. 5d).

The wide and solvent-accessible periplasmic half-channel is most likely filled with water molecules, which will immediately form a hydration shell around the Na^+, making this step energetically favourable. According to this model the subsequent final electron transfer from $riboflavin_{NqrB}$ to ubiquinone is not essential for Na^+ translocation.

The structure of Na^+-NQR of human pathogen *Vibrio cholerae* presented here suggests a new mechanism for the coupling between redox reactions and ion translocation events in a respiratory complex. Na^+-NQR is a central component of the energy conservation system in a plethora of pathogenic bacteria. This structure may serve as the basis for the development of new antibiotics against the worldwide increase in antibiotic-resistant pathogens.

Online Content Methods, along with any additional Extended Data display items and Source Data, are available in the online version of the paper; references unique to these sections appear only in the online paper.

Received 11 August; accepted 24 October 2014.

1. Mitchell, P. Coupling of phosphorylation to electron and hydrogen transfer by a chemi-osmotic type of mechanism. *Nature* **191,** 144–148 (1961).
2. Pfenninger-Li, X. D., Albracht, S. P., van Belzen, R. & Dimroth, P. NADH:ubiquinone oxidoreductase of *Vibrio alginolyticus*: purification, properties, and reconstitution of the Na^+ pump. *Biochemistry* **35,** 6233–6242 (1996).

3. Juárez, O., Nilges, M. J., Gillespie, P., Cotton, J. & Barquera, B. Riboflavin is an active redox cofactor in the Na^+-pumping NADH: quinone oxidoreductase (Na^+-NQR) from *Vibrio cholerae*. *J. Biol. Chem.* **283,** 33162–33167 (2008).
4. Casutt, M. S. *et al.* Localization of ubiquinone-8 in the Na^+-pumping NADH:quinone oxidoreductase from *Vibrio cholerae*. *J. Biol. Chem.* **286,** 40075–40082 (2011).
5. Häse, C. C. & Mekalanos, J. J. Effects of changes in membrane sodium flux on virulence gene expression in *Vibrio cholerae*. *Proc. Natl Acad. Sci. USA* **96,** 3183–3187 (1999).
6. Müller, V., Imkamp, F., Biegel, E., Schmidt, S. & Dilling, S. Discovery of a ferredoxin:NAD^+-oxidoreductase (Rnf) in *Acetobacterium woodii*. *Ann. NY Acad. Sci.* **1125,** 137–146 (2008).
7. Holm, L. & Rosenstrom, P. Dali server: conservation mapping in 3D. *Nucleic Acids Res.* **38,** W545–W549 (2010).
8. Baradaran, R., Berrisford, J. M., Minhas, G. S. & Sazanov, L. A. Crystal structure of the entire respiratory complex I. *Nature* **494,** 443–448 (2013).
9. Reyes-Prieto, A., Barquera, B. & Juárez, O. Origin and evolution of the sodium-pumping NADH: ubiquinone oxidoreductase. *PLoS ONE* **9,** e96696 (2014).
10. Nedielkov, R., Steffen, W., Steuber, J. & Möller, H. M. NMR reveals double occupancy of quinone-type ligands in the catalytic quinone binding site of the Na^+-translocating NADH:quinone oxidoreductase from *Vibrio cholerae*. *J. Biol. Chem.* **288,** 30597–30606 (2013).
11. Levin, E. J. *et al.* Structure and permeation mechanism of a mammalian urea transporter. *Proc. Natl Acad. Sci. USA* **109,** 11194–11199 (2012).
12. Khademi, S. *et al.* Mechanism of ammonia transport by Amt/MEP/Rh: structure of AmtB at 1.35 Å. *Science* **305,** 1587–1594 (2004).
13. Andrade, S. L., Dickmanns, A., Ficner, R. & Einsle, O. Crystal structure of the archaeal ammonium transporter Amt-1 from *Archaeoglobus fulgidus*. *Proc. Natl Acad. Sci. USA* **102,** 14994–14999 (2005).
14. Wacker, T., Garcia-Celma, J. J., Lewe, P. & Andrade, S. L. Direct observation of electrogenic NH_4^+ transport in ammonium transport (Amt) proteins. *Proc. Natl Acad. Sci. USA* **111,** 9995–10000 (2014).
15. Juárez, O., Athearn, K., Gillespie, P. & Barquera, B. Acid residues in the transmembrane helices of the Na^+-pumping NADH:quinone oxidoreductase from *Vibrio cholerae* involved in sodium translocation. *Biochemistry* **48,** 9516–9524 (2009).
16. Juárez, O., Morgan, J. E., Nilges, M. J. & Barquera, B. Energy transducing redox steps of the Na^+-pumping NADH:quinone oxidoreductase from *Vibrio cholerae*. *Proc. Natl Acad. Sci. USA* **107,** 12505–12510 (2010).
17. Casutt, M. S., Schlosser, A., Buckel, W. & Steuber, J. The single NqrB and NqrC subunits in the Na^+-translocating NADH:quinone oxidoreductase (Na^+-NQR) from *Vibrio cholerae* each carry one covalently attached FMN. *Biochim. Biophys. Acta* **1817,** 1817–1822 (2012).
18. Duffy, E. B. & Barquera, B. Membrane topology mapping of the Na^+-pumping NADH:quinone oxidoreductase from *Vibrio cholerae* by PhoA/GFP fusion analysis. *J. Bacteriol.* **188,** 8343–8351 (2006).
19. Bertsova, Y. V. *et al.* Alternative pyrimidine biosynthesis protein ApbE is a flavin transferase catalyzing covalent attachment of FMN to a threonine residue in bacterial flavoproteins. *J. Biol. Chem.* **288,** 14276–14286 (2013).
20. Casutt, M. S. *et al.* Localization and function of the membrane-bound riboflavin in the Na^+-translocating NADH:quinone oxidoreductase (Na^+-NQR) from *Vibrio cholerae*. *J. Biol. Chem.* **285,** 27088–27099 (2010).
21. Terwilliger, T. C., Klei, H., Adams, P. D., Moriarty, N. W. & Cohn, J. D. Automated ligand fitting by core-fragment fitting and extension into density. *Acta Crystallogr. D* **62,** 915–922 (2006).
22. Page, C. C., Moser, C. C., Chen, X. & Dutton, P. L. Natural engineering principles of electron tunnelling in biological oxidation-reduction. *Nature* **402,** 47–52 (1999).
23. Tao, M., Casutt, M. S., Fritz, G. & Steuber, J. Oxidant-induced formation of a neutral flavosemiquinone in the Na^+-translocating NADH:quinone oxidoreductase (Na^+-NQR) from *Vibrio cholerae*. *Biochim. Biophys. Acta* **1777,** 696–702 (2008).
24. Zhang, Z. *et al.* Electron transfer by domain movement in cytochrome bc_1. *Nature* **392,** 677–684 (1998).
25. Verkhovsky, M. I. *et al.* Sodium-dependent movement of covalently bound FMN residue(s) in Na^+-translocating NADH:quinone oxidoreductase. *Biochemistry* **51,** 5414–5421 (2012).
26. Steuber, J. *et al.* Central role of the Na^+-translocating NADH:quinone oxidoreductase (Na^+-NQR) in sodium bioenergetics of *Vibrio cholerae*. *Biol. Chem.* **395,** 1389–1399 (2014).
27. Rich, P. R., Meunier, B. & Ward, F. B. Predicted structure and possible ionmotive mechanism of the sodium-linked NADH-ubiquinone oxidoreductase of *Vibrio alginolyticus*. *FEBS Lett.* **375,** 5–10 (1995).
28. Bogachev, A. V., Bertsova, Y. V., Aitio, O., Permi, P. & Verkhovsky, M. I. Redox-dependent sodium binding by the Na^+-translocating NADH:quinone oxidoreductase from *Vibrio harveyi*. *Biochemistry* **46,** 10186–10191 (2007).
29. Verkhovsky, M. I. & Bogachev, A. V. Sodium-translocating NADH:quinone oxidoreductase as a redox-driven ion pump. *Biochim. Biophys. Acta* **1797,** 738–746 (2010).
30. Bogachev, A. V., Belevich, N. P., Bertsova, Y. V. & Verkhovsky, M. I. Primary steps of the Na^+-translocating NADH:ubiquinone oxidoreductase catalytic cycle resolved by the ultrafast freeze-quench approach. *J. Biol. Chem.* **284,** 5533–5538 (2009).
31. Bogachev, A. V., Bertsova, Y. V., Ruuge, E. K., Wikstrom, M. & Verkhovsky, M. I. Kinetics of the spectral changes during reduction of the Na^+-motive NADH:quinone oxidoreductase from *Vibrio harveyi*. *Biochim. Biophys. Acta* **1556,** 113–120 (2002).
32. Zhu, W. & Becker, D. F. Flavin redox state triggers conformational changes in the PutA protein from *Escherichia coli*. *Biochemistry* **42,** 5469–5477 (2003).
33. Leung, K. K. & Shilton, B. H. Chloroquine binding reveals flavin redox switch function of quinone reductase 2. *J. Biol. Chem.* **288,** 11242–11251 (2013).
34. Bogachev, A. V., Murtazina, R. A. & Skulachev, V. P. The Na^+/e^- stoichiometry of the Na^+-motive NADH:quinone oxidoreductase in *Vibrio alginolyticus*. *FEBS Lett.* **409,** 475–477 (1997).

Acknowledgements We thank the staff at beamlines X06SA and X06DA at Swiss Light Source for excellent support. This work was supported by contract research 'Methoden in den Lebenswissenschaften' of the Baden-Württemberg Stiftung P-LS-Meth/4 (to J.S. and G.F.), and by the Deutsche Forschungsgemeinschaft grant FR 1321/3-1 (to J.S.) and grant FR 1488/3-2 (to G.F.). We thank Y. Obermaier for expression and preparation of Na^+-NQR.

Author Contributions J.S., G.F. and T.V. developed expression constructs; J.S. and M.S.C. developed purification procedures; T.V., M.S.C. and G.V. expressed the protein; M.S.C., G.V. and G.F. purified the entire complex or single subunits; M.S.C., G.V. and G.F. performed crystallization, crystal harvesting and data collection. G.F. and K.D. performed data processing and determination of phases. G.F. performed model building and refinement. G.F. prepared the figures. G.F. and J.S. wrote the manuscript.

Author Information Coordinates and structure factors for the entire complex of Na^+-NQR and of individual subunits $NqrA_{1–377}$, $NqrC_{33–257}$ and $NqrF_{129–408}$ have been deposited in the Protein Data Bank. The PDB accession codes are 4P6V (entire NQR complex), 4U9O (subunit NqrA, crystal 1), 4U9Q (subunit NqrA, crystal 2), 4U9S (subunit NqrC), and 4U9U (subunit NqrF). Reprints and permissions information is available at www.nature.com/reprints. The authors declare no competing financial interests. Readers are welcome to comment on the online version of the paper. Correspondence and requests for materials should be addressed to G.F. (guenter.fritz@uniklinik-freiburg.de).

METHODS

Na^+-NQR was expressed, purified and crystallized as described previously[35]. Selenomethionine (SeMet)-labelled Na^+-NQR was obtained by growth in minimal medium with L-selenomethionine as sole source for methionine as described in the following. From glycerol stocks, *V. cholerae* O395-N1 Δnqr[36], transformed with pNQR1[23] or pNqr-PreScission (this work), was cultivated on LB plates containing 10 g l^{-1} tryptone, 5 g l^{-1} yeast extract, 10 g l^{-1} NaCl, 15 g l^{-1} bactoagar, 50 mM potassium phosphate (KP_i) pH 8.5, 10 mM glucose, 50 μg ml^{-1} streptomycin and 200 μg ml^{-1} ampicillin. A single colony was used to inoculate 5 ml LB (composition as described above, but without bactoagar), and cells were grown for 16 h at 37 °C, 220 r.p.m. shaking. Growth was continued in 150 ml LB (inoculum size: 3 ml) for 4 h at 37 °C, 220 r.p.m. shaking. 15 ml were used to inoculate 1 litre Se-Met minimal medium (in a 5 l Erlenmeyer flask) consisting of 15 mM $(NH_4)_2SO_4$, 50 mM KP_i pH 8.5, 0.8 μM $FeSO_4$, alanine, arginine, glycine, glutamine, histidine, isoleucine, leucine, lysine, proline, serine, threonine, valine, asparagine, aspartic acid, cysteine, glutamic acid, phenylalanine, tyrosine, hypoxanthine, uracil (40 μg ml^{-1} of each), tryptophan (20 μg ml^{-1}), *p*-hydroxybenzoic acid (4 μg ml^{-1}), biotin, nicotinamide, thiamine (2 μg ml^{-1} of each), riboflavin (1 μg ml^{-1}), 1 mM $MgSO_4$, 10 mM glucose, 1% glycerol (v/v), 1% DMSO (v/v), 170 mM NaCl, 50 μg ml^{-1} streptomycin, 200 μg ml^{-1} ampicillin and L-selenomethionine (50 μg ml^{-1}). At 37 °C, 150 r.p.m. shaking, cells were grown to an optical density at 600 nm of 1.0. Na^+-NQR production was induced by adding 5 ml 20% L-arabinose, and expression was continued for 12 h at 30 °C, 110 r.p.m. shaking. The culture was cooled on ice, cells were collected by centrifugation (10,000*g*, 30 min, 4 °C), washed in 100 ml lysis buffer (500 mM NaCl, 50 mM sodium phosphate pH 8.0), suspended in lysis buffer (1 g wet weight of cells per ml of buffer), frozen in liquid nitrogen and stored at −80 °C. After an expression phase of 12 h, cultures in selenomethionine minimal medium typically reached an optical density at 600 nm of 1.8. Typical yields were 4.5 g cells wet weight per litre of culture. The (SeMet)-labelled Na^+-NQR was purified as described[35]. Diffraction data were collected at the Swiss Light Source, beamline X06SA equipped with a PILATUS 6 M detector. All diffraction data were integrated using XDS[37]. A Ta_6Br_{12} derivative was obtained by soaking native crystals overnight in 2 mM Ta_6Br_{12} (Extended Data Table 1). Initial phases were calculated with SHARP[38]. After solvent flattening with Solomon[39] or DM[40] the resulting electron density map was of sufficient quality to build about 18 transmembrane helices. However, it was not possible to place any further structural elements into the experimental map. Further phase information was obtained from a SeMet derivative (Extended Data Table 1). The initial transmembrane helix model was used as a search model in a combined molecular replacement SAD approach using Phaser[41]. A total of 58 out of 70 Se sites were found in the first trial and the resulting electron density map was of good quality. Several cycles of model building with COOT[42] and SAD phasing were performed. A large part of the sequence of the transmembrane helices could be assigned using the positions of the Se sites in methionine residues as marker. The previously proposed symmetric and inverted topology of NqrD and NqrE helped to assign the helices to the different subunits. However, several transmembrane helices of NqrB contain no methionine and it was not possible to trace the sequence throughout the ten transmembrane helices. We therefore performed sequence-based searches for structures homologous to the different subunits of Na^+-NQR using the HHPred server[43] that utilizes hidden Markov models. NqrB was predicted to be structurally homologous to the urea transporter[11] and the structure could be aligned with the transmembrane helices guiding the tracing of the sequence. The low resolution of the experimental map allowed the unambiguous placement of side chains for methionine or tryptophan residues only. We therefore produced recombinantly several soluble domains of NqrA, NqrC and NqrF, crystallized these proteins separately and solved their structures at 1.60 Å, 1.70 Å and 1.55 Å[44,45]. The structures of these subunits were placed into the low resolution experimental map by molecular replacement using MOLREP[46], and their localization in the complex was verified by the positions of the methionine residues indicated by the Se positions. Refinement was performed using Refmac5[47] and with phenix.refine[48] using the high-resolution structures of NqrA, NqrC and NqrF as reference models. The high-resolution limits were established by paired-refinement[49]. Several cycles of manual rebuilding and refinement allowed finally the placement of 1,774 residues and 6 cofactors and the structure was refined at 3.5 Å resolution to a final R_{work} = 24.6% and R_{free} = 27.6% (Extended Data Table 1) with good stereochemistry parameters compared to other structures determined at this resolution. The refined model at 3.5 Å resolution showed no substantial deviation from the high resolution structural data of the single subunits (Extended Data Table 4). Analysis with MolProbity[50] shows that 90.2% of the residues in Na^+-NQR are in the favourable regions of the Ramachandran plot with 7% in the allowed regions, and 2.8% outliers. Most of the outliers are located in the integral membrane subunits or areas where the electron density was less well defined. Cavities and putative channels were calculated with CAVER[51], and surface potential was calculated with APBS[52]. All figures were prepared with PyMol[53].

35. Casutt, M. S., Wendelspiess, S., Steuber, J. & Fritz, G. Crystallization of the Na^+-translocating NADH:quinone oxidoreductase from *Vibrio cholerae*. *Acta Crystallogr. F* **66,** 1677–1679 (2010).
36. Barquera, B. *et al.* Purification and characterization of the recombinant Na^+-translocating NADH:quinone oxidoreductase from *Vibrio cholerae*. *Biochemistry* **41,** 3781–3789 (2002).
37. Kabsch, W. XDS. *Acta Crystallogr. D* **66,** 125–132 (2010).
38. Bricogne, G., Vonrhein, C., Flensburg, C., Schiltz, M. & Paciorek, W. Generation, representation and flow of phase information in structure determination: recent developments in and around SHARP 2.0. *Acta Crystallogr. D* **59,** 2023–2030 (2003).
39. Abrahams, J. P. & Leslie, A. G. Methods used in the structure determination of bovine mitochondrial F_1 ATPase. *Acta Crystallogr. D* **52,** 30–42 (1996).
40. Cowtan, K. Error estimation and bias correction in phase-improvement calculations. *Acta Crystallogr. D* **55,** 1555–1567 (1999).
41. McCoy, A. J. *et al. Phaser* crystallographic software. *J. Appl. Cryst.* **40,** 658–674 (2007).
42. Emsley, P., Lohkamp, B., Scott, W. G. & Cowtan, K. Features and development of Coot. *Acta Crystallogr. D* **66,** 486–501 (2010).
43. Söding, J., Biegert, A. & Lupas, A. N. The HHpred interactive server for protein homology detection and structure prediction. *Nucleic Acids Res.* **33,** W244–W248 (2005).
44. Tao, M. *et al.* Crystallization of the NADH-oxidizing domain of the Na^+-translocating NADH:ubiquinone oxidoreductase from *Vibrio cholerae*. *Acta Crystallogr. F* **62,** 110–112 (2006).
45. Vohl, G. *et al.* Crystallization and preliminary analysis of the NqrA and NqrC subunits of the Na^+-translocating NADH:ubiquinone oxidoreductase from *Vibrio cholerae*. *Acta Crystallogr. F* **70,** 987–992 (2014).
46. Vagin, A. & Teplyakov, A. Molecular replacement with MOLREP. *Acta Crystallogr. D* **66,** 22–25 (2010).
47. Murshudov, G. N. *et al.* REFMAC5 for the refinement of macromolecular crystal structures. *Acta Crystallogr. D* **67,** 355–367 (2011).
48. Headd, J. J. *et al.* Use of knowledge-based restraints in phenix.refine to improve macromolecular refinement at low resolution. *Acta Crystallogr. D* **68,** 381–390 (2012).
49. Karplus, P. A. & Diederichs, K. Linking crystallographic model and data quality. *Science* **336,** 1030–1033 (2012).
50. Chen, V. B. *et al.* MolProbity: all-atom structure validation for macromolecular crystallography. *Acta Crystallogr. D* **66,** 12–21 (2010).
51. Chovancova, E. *et al.* CAVER 3.0: a tool for the analysis of transport pathways in dynamic protein structures. *PLOS Comput. Biol.* **8,** e1002708 (2012).
52. Baker, N. A., Sept, D., Joseph, S., Holst, M. J. & McCammon, J. A. Electrostatics of nanosystems: application to microtubules and the ribosome. *Proc. Natl Acad. Sci. USA* **98,** 10037–10041 (2001).
53. The PyMOL Molecular Graphics System, v. 1.3r1 (Schrödinger, LLC, 2010).
54. Sääf, A., Johansson, M., Wallin, E. & von Heijne, G. Divergent evolution of membrane protein topology: the *Escherichia coli* RnfA and RnfE homologues. *Proc. Natl Acad. Sci. USA* **96,** 8540–8544 (1999).
55. Bogachev, A. V., Bertsova, Y. V., Bloch, D. A. & Verkhovsky, M. I. Thermodynamic properties of the redox centres of Na^+-translocating NADH:quinone oxidoreductase. *Biochemistry* **45,** 3421–3428 (2006).
56. Bogachev, A. V. *et al.* Redox properties of the prosthetic groups of Na^+-translocating NADH:quinone oxidoreductase. 1. Electron paramagnetic resonance study of the enzyme. *Biochemistry* **48,** 6291–6298 (2009).

Extended Data Figure 1 | Sequence alignment of the integral membrane subunit NqrB from different organism with the corresponding subunits of the RNF complex. The localization of transmembrane helices is indicated by cylinders. Connecting loops located in the cytoplasm are shown in red, connecting loops located in the periplasm in blue. Thr 236 covalently binding the FMN, and Asp 346 located in the proposed Na^+ channel are indicated by arrows.

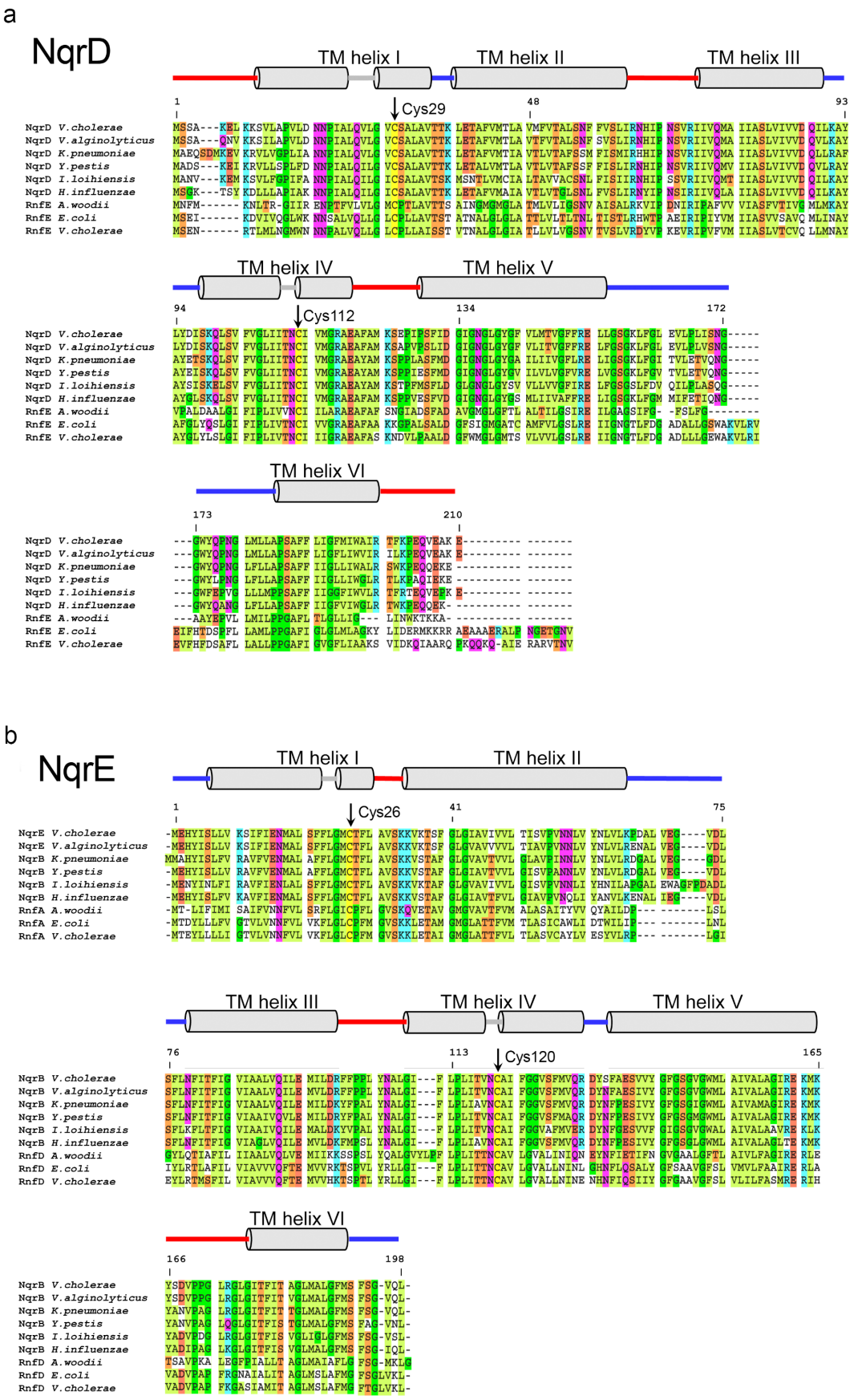

Extended Data Figure 2 | Sequence alignment of the integral membrane subunits NqrD and NqrE from different organism with the corresponding subunits of the RNF complex. a, **b**, The localization of transmembrane helices is indicated by cylinders; connecting loops located in the cytoplasm are shown in red, connecting loops located in the periplasm in blue. Cys residues in NqrD (**a**) and NqrE (**b**) coordinating the Fe are indicated by arrows.

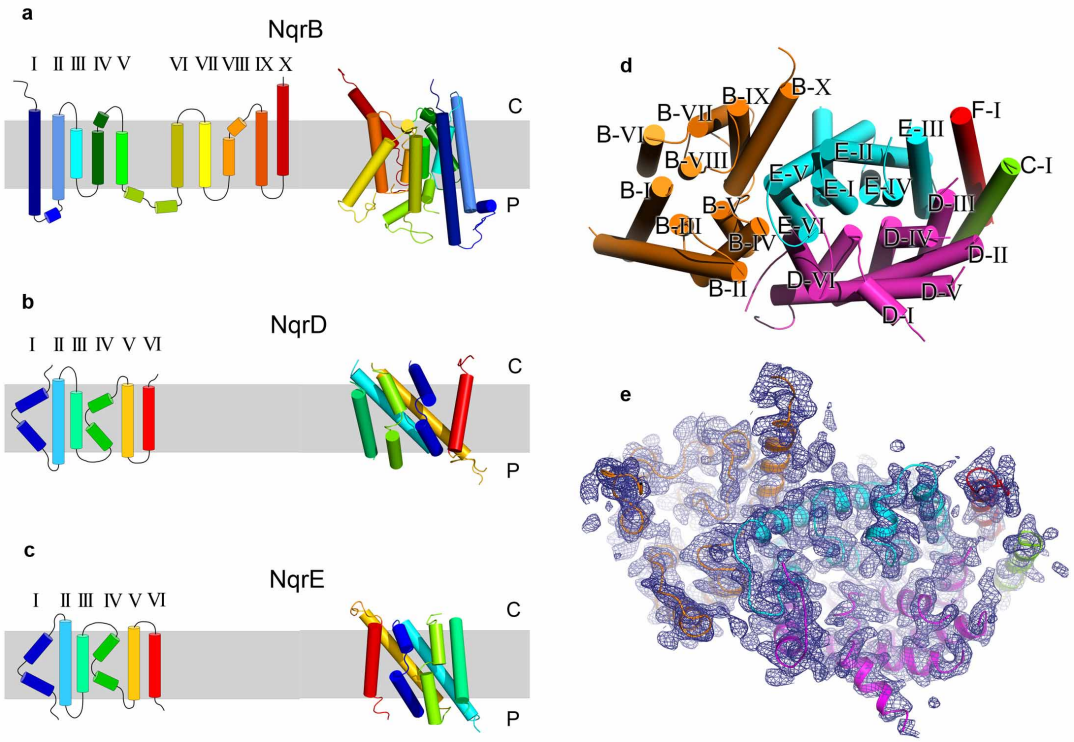

Extended Data Figure 3 | Topology of the transmembrane subunits NqrB, NqrD, and NqrE and arrangement of transmembrane helices. **a**–**c**, The schematic topology of the transmembrane helices of NqrB, NqrC and NqrD is shown on the left hand side and the corresponding structure on the right hand side. The membrane plane is indicated in grey and the cytoplasmic aspect is marked by C and the periplasmic aspect by P. **a**, NqrB contains ten transmembrane helices which can be divided into a N-terminal domain comprising helices I–V and a C-terminal domain comprising helices VI–X, which exhibit an inverted topology. Both domains are connected by a long periplasmic linker. The domains exhibit an inverted topology and align with an r.m.s.d. of 3.3 Å over 113 Cα positions. **b**, **c**, NqrD and NqrE each comprise six helices exhibiting an inverted topology. Helix I and helix IV of both subunits are composed of two half helices. Such an inverted topology had been predicted based on the sequence information[54]. **d**, Top view from the cytoplasmic side onto the transmembrane helices of subunits NqrB, NqrC, NqrD, NqrE and NqrF. There are a total of 24 transmembrane helices. NqrD and NqrE form a central symmetrical unit. Subunit NqrB resides on one side of the NqrD–E unit whereas the single transmembrane helices from NqrC and NqrF reside on the opposed side. NqrB is closely attached to NqrE via helices V and VI from NqrE and IV, V, IX and X from NqrB, forming an interaction surface of 1,280 $Å^2$, whereas NqrD exhibits a much smaller contact area to NqrB via helices VI from NqrD and IV and V from NqrB, covering 335 $Å^2$. The transmembrane helices of NqrC and NqrF are close to each other but interact with different subunits: the transmembrane helix of NqrC forms contacts with helix III of NqrD, whereas the transmembrane helix of NqrF interacts with helix III of NqrE. **e**, Top view of the transmembrane part of Na^+-NQR and $2F_o - F_c$ electron density displayed at a contour level of 1.0σ. The map coefficients were sharpened by a *B*-factor of −80 $Å^2$.

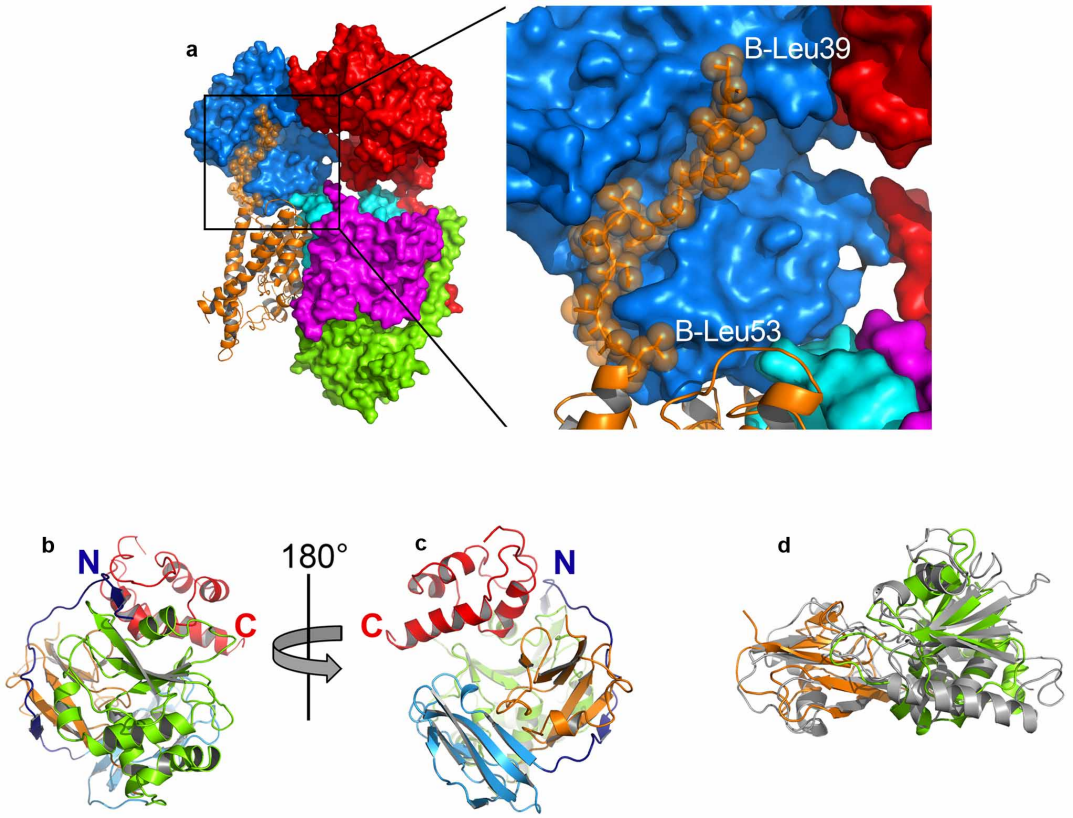

Extended Data Figure 4 | Subunit NqrA. **a**, Interactions of NqrA with other subunits in the Na^+-NQR complex. The subunits of Na^+-NQR are shown in different colours: NqrA in blue, NqrB in orange, NqrC in green, NqrD in magenta, NqrE in cyan, and NqrF in red. Subunit B is shown as cartoon and all other subunits as surface representation. The C-terminal domain of NqrA located proximal to the membrane forms minor contacts with the integral membrane subunit NqrB via the NqrA residues 376–379 and 425–428, located in two short loops. A long N-terminal stretch of NqrB encompassing residues 39–53 lies in a groove of NqrA interacting over a total area of 820 $Å^2$ and anchoring NqrA to the membrane subunits. The residues shown as transparent van der Waals spheres fill almost the entire groove of NqrA. At the C terminus of NqrB, transmembrane helix 10 is elongated and protrudes into the cytoplasm, forming contacts with the C-terminal domain and the Rossmann-fold domain of NqrA, covering a total area of 430 $Å^2$. **b**, **c**, NqrA is composed of four domains, an N-terminal domain similar to a biotin carboxyl carrier domain (blue, residues 28–100), a Rossmann-fold domain (green, residues 102–254), an ubiquitin-like domain (orange, residues 258–329), and a C-terminal helical domain (red, residues 376–446). The N-terminal residues 1–27 wrap around the Rossmann-fold domain and the ubiquitin-like domain and form two short β-strands that align with β-sheets of both domains, respectively. The C-terminal helical domain of NqrA shows similarity to a 2[4Fe–4S] cluster ferredoxin fold like for example, in fumarate reductase (PDB code 1KF6), but does not contain a FeS centre. Consistently, the Cys residues required for FeS coordination are not present in NqrA. **d**, Structural alignment of NqrA with Nqo1 from complex I (grey). The proteins align with an r.m.s.d. of 3.9 Å over 234 Cα positions. NqrA comprises a deep solvent-accessible cavity that is formed by residues of the Rossmann-fold domain and the ubiquitin-like domain that is large enough to accommodate ubiquinone. In case of Nqo1 of complex I the corresponding cavity harbours the isoalloxazine moiety of the FMN cofactor.

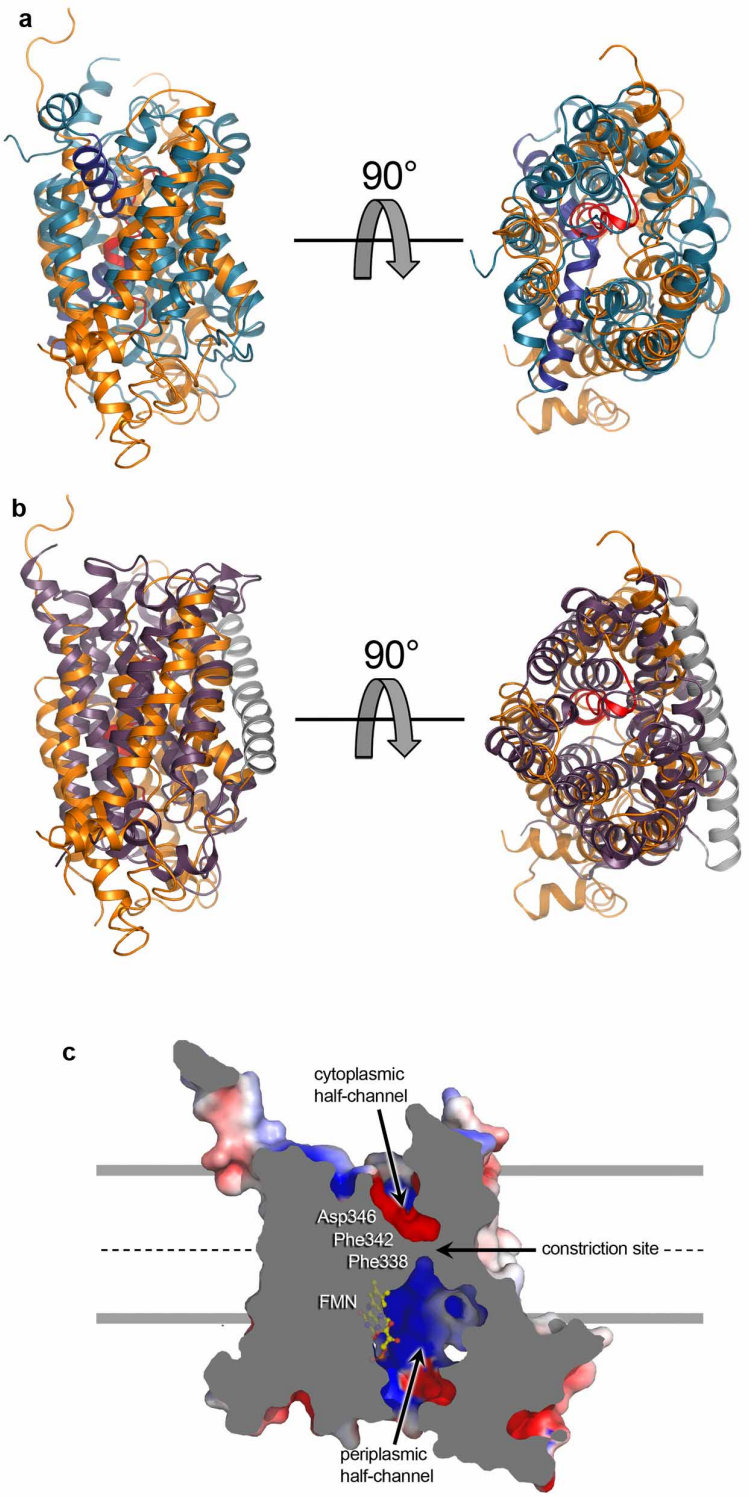

Extended Data Figure 5 | A putative Na^+ channel in subunit NqrB. **a**, **b**, Structural alignments of NqrB with urea transporter and ammonium transporter are shown. In NqrB the central helices I, III, VI and VIII form a membrane-spanning channel. Some backbone carbonyls, for example, from Val 161, Ile 164, Leu 168 from helix III deviate notably from the ideal geometry and point inwards the channel. Such a distortion indicates a putative involvement in Na^+ coordination. **a**, The left hand side represents the side view and the right hand side the top view of NqrB (orange) aligned with bovine urea transporter (blue). Helix VIII of NqrB carrying residues forming the constriction is shown in red. The gating helices of urea transporter, which have no corresponding helices in NqrB, are depicted in dark blue. **b**, Structural alignment of NqrB (orange) with ammonium transporter from *Archaeoglobus fulgidus*. The outer helix of ammonium transporter that has no homologous helix in NqrB is shown in grey. The high structural similarity of NqrB with urea and ammonium transporter shows that the subunit preserved the basic architecture of a transporter, but has acquired an additional and completely different function as a redox protein. These structural rearrangements in the periplasmic aspect of NqrB required to embed the FMN cofactor might have contributed to the closure of the channel. **c**, Cross section through NqrB. The surface is coloured according to the electrostatic surface potential. The cytoplasmic half channel exhibits a negative surface charge (red) whereas the periplasmic half channel is positively charged (blue). The localization of residues Phe 338, Phe 342 and Asp 346 is indicated. The constriction is located halfway through the membrane. The borders of the cytoplasmic membrane are indicated by grey lines.

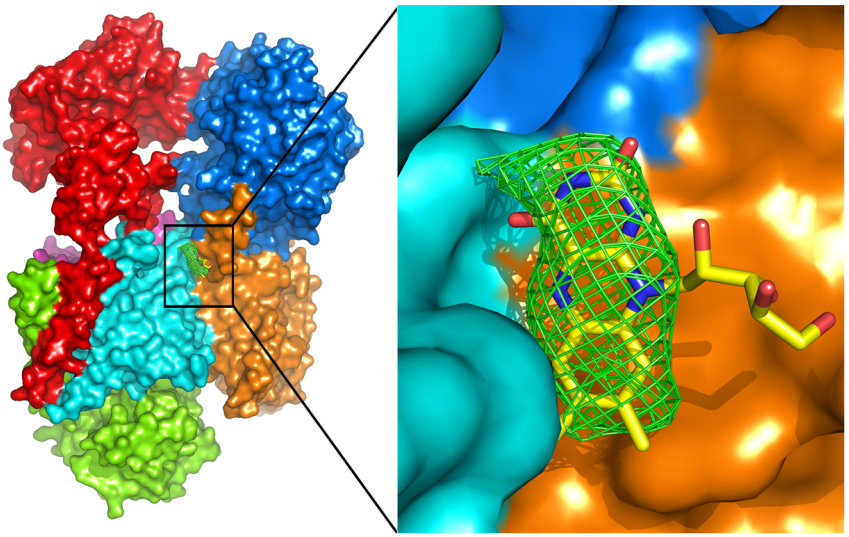

Extended Data Figure 6 | Localization of riboflavin. A large patch of $F_o - F_c$ density was observed between NqrB (orange) and NqrE (cyan) and assigned to the riboflavin. The isoalloxazine moiety of riboflavin fits well into the $F_o - F_c$ density. Several interactions with the protein matrix can stabilize the riboflavin. The flavin is stacked between the side chain of Val 399 and the CB, CG of Glu 402 of NqrB on one side (*Si* side) and the side chain of Phe 39 of NqrE on the opposed side (*Re*-side). Moreover, the imidazole of His 398 of NqrB on the *Si*-side can form a hydrogen bond to N5 of isoalloxazine.

Extended Data Table 1 | Data collection, phasing and refinement statistics

	Native	Ta_6Br_{12}	Se Met	Fe
Data collection				
X-ray source	SLS, X06SA	SLS, X06SA	SLS, X06SA	SLS, X06SA
Wavelength (Å)	0.90	1.225	0.9797 (peak)	1.736 (peak)
Total rotation range	720°	1200°	4720°	1600°
Space group	$P2_1$	$P2_1$	$P2_1$	$P2_1$
Unit-cell parameters				
a, *b*, *c* (Å)	95.3, 143.4, 104.5	96.7, 151.3, 106.1	96.2, 150.8, 108.2	95.7, 150.3, 107.5
α, β, γ (°)	90, 110.9, 90	90,111.5, 90	90, 111.8, 90	90, 111.6, 90
Resolution (Å)	50-3.5 (3.7-3.5)	50-4.2 (4.4-4.2)	50-3.8 (4.0-3.8)	50-4.0 (4.2-4.0)
R_{merge} (%)	17.1 (563.8)	7.8 (174.5)	12.6 (383.4)	6.7 (135.1)
R_{meas} (%)	17.8 (584.9)	8.2 (182.5)	12.8 (387.5)	6.9 (139.9)
R_{pim} (%)	4.8 (156.4)	2.4 (53.7)	1.8 (56.8)	1.7 (36.0)
$CC_{1/2}$	0.999 (0.411)	1.000 (0.568)	1.000 (0.362)	1.000 (0.496)
I/σ(I)	10.9 (0.86)	11.9 (1.35)	18.4 (1.4)	14.4 (2.0)
Completeness (%)	99.7 (99.8)	99.4 (99.4)	99.5 (99.5)	99.5 (98.9)
Multiplicity	13.7 (14.0)	11.7 (11.6)	46.6 (46.6)	15.5 (15.1)
No. molecules per ASU	1	1	1	1
Solvent content (%)	59.9	62.9	63.2	62.7
Refinement				
Resolution (Å)	50-3.5 (3.7-3.5)	50-4.2 (4.4-4.2)	50-3.8 (4.0-3.8)	50-4.0 (4.2-4.0)
No. of reflections	452,674 (70,668)	477,442 (62,286)	2,588,229 (370,515)	726,668 (95,391)
No. of unique reflections	33,122 (5,032)	40,704 (5,337)	55,473 (7,935)	46,881 (6,336)
R_{work} (%)	24.6 (35.2)			
Rf_{ree} (%)	27.6 (38.1)			
No. atoms Protein Ligand/ion	13,607 13,461 146			
Mean B-factors (Å^2) Protein Ligand/ion	167.7 167.5 183.7			
R.m.s. deviations Bond lengths (Å) Bond angles (°)	 0.011 1.12			
MolProbity overall score Clashscore	2.99 14.14			
Ramachandran plot (%) (favoured/allowed/outliers)	 (90.2/7.0/2.8)			

Extended Data Table 2 | Fe anomalous map peak heights

Crystal No.	Wavelength (Å)	Anomalous peak height at position of $[2Fe\text{-}2S]_{NqrF}$	Anomalous peak height at position of $Fe_{NqrD/E}$
1	1.7268 (remote high)	9.1	11.8
1	1.7360 (peak)	8.4	13.2
1	1.7428 (inflection)	8.4	13.7
1	1.7463 (remote low)	3.0	2.7
2	1.7287 (remote high)	5.3	6.0
2	1.7360 (peak)	7.6	9.3
2	1.7428 (inflection)	4.7	3.6
2	1.7463 (remote low)	0	0

To prove the identity of Fe causing the strong peak in the anomalous map localized in subunits NqrD–E, we recorded data sets at different wavelengths close to the K–absorption edge of Fe. The wavelengths were chosen according to a fluorescence scan around the Fe K–edge. The resulting anomalous peak heights at the different wavelengths are similar for both, the $[2Fe–2S]_{NqrF}$ site and the $Fe_{NqrD–E}$ site. The maximal peak height is observed at a wavelength corresponding to the peak of absorption. Changing the wavelength towards lower energy results in a sharp drop and no anomalous signal is observed at a wavelength where Fe does not absorb. Multiple fluorescence scans on different crystals revealed no further presence of any metal ion in Na^+-NQR. The similar peak height at the $[2Fe–2S]_{NqrF}$ site and $Fe_{NqrD–E}$ site might be attributed to conformational flexibility of subunit NqrF as indicated by higher *B*-factors compared to the integral membrane subunits. Such flexibility will result in a weaker anomalous signal from the $[2Fe–2S]_{NqrF}$ centre.

Extended Data Table 3 | Redox cofactor distances

Redox cofactor pair	Edge-to-edge (Å)	Centre-to-centre (Å) Atom ID	$E^{0'}$ (mv) *
FAD_{NqrF} / $[2Fe\text{-}2S]_{NqrF}$	9.8	16.0 (FAD-N5 / [2Fe-2S]-Fe1)	-200 / -275
$[2Fe\text{-}2S]_{NqrF}$ / $Fe_{NqrD\backslash E}$	33.2	36.4 ([2Fe-2S]-Fe1 / $Fe_{NqrD\backslash E}$)	-200 / n.d.
$[2Fe\text{-}2S]_{NqrF}$ / Riboflavin	29.4	34.6 ([2Fe-2S]-Fe1 / Riboflavin-N5)	-200 / -10
$Fe_{NqrD\backslash E}$ / FMN_{NqrC}	7.9	13.2 ($Fe_{NqrD\backslash E}$ / FMN_{NqrC}–N5)	n.d. / -190
$Fe_{NqrD\backslash E}$ / Riboflavin	30.8	32.8 ($Fe_{NqrD\backslash E}$ / Riboflavin–N5)	n.d. / -10
$Fe_{NqrD\backslash E}$ / FMN_{NqrB}	29.6	32.9 ($Fe_{NqrD\backslash E}$ / FMN_{NqrB}–N5)	n.d. / -130
FMN_{NqrC} / FMN_{NqrB}	21.4	27.2 (FMN_{NqrC}–N5 / FMN_{NqrB}–N5)	-190 / -130
FMN_{NqrB} / Riboflavin	29.3	32.7 (FMN_{NqrB}–N5 / Riboflavin–N5)	-190 / -130

* The values are taken from refs 55 and 56.

Extended Data Table 4 | r.m.s.d. deviations between subunits in NQR complex and the structures of the individual subunits

Na^+-NQR / subunit pair	No. Cα	R.M.S.D. (Å)
Na^+-NQR / $NqrA_{1\text{-}377}$ SG $C222_1$ (PDB 4U9O)	298	0.82
Na^+-NQR / $NqrA_{1\text{-}377}$ SG $P2_1$ (PDB 4U9Q)	293	3.86
Na^+-NQR / $NqrC_{33\text{-}257}$ (PDB 4U9S)	218	1.01
Na^+-NQR / $NqrF_{129\text{-}408}$ (PDB 4U9U)	279	0.69

The high-resolution structures of the individual subunits deviate only to a minor extent from the corresponding parts in the entire complex. Largest differences are observed for $NqrA_{1\text{–}377}$, which was crystallized in two different space groups. $NqrA_{1\text{–}377}$, crystallized in space group $C222_1$, displays a r.m.s.d. of 0.82 Å, whereas $NqrA_{1\text{–}377}$, crystallized in space group $P2_1$, exhibits a r.m.s.d. of 3.86 Å. This deviation originates mainly from a different conformation in the NqrA region 213–235 and from different conformations of two loops encompassing residues 155–161 and 292–297, respectively. In the structure of the entire NqrA in the NQR complex this region is in contact with the C-terminal domain of NqrA and forms a short α-helix (residues 219–229), whereas this region forms an extended loop stabilized by crystal contacts in $NqrA_{1\text{–}377}$ in space group $P2_1$. In crystals of $NqrA_{1\text{–}377}$ in space group $C222_1$ this region was completely unordered and could not be resolved in the electron density.